

Two distinct mechanisms for loss of thioredoxin-binding protein-2 in oxidative stress-induced renal carcinogenesis

Khokon K Dutta¹, Yumiko Nishinaka^{2,3}, Hiroshi Masutani^{2,3}, Shinya Akatsuka¹, Than T Aung¹, Tomoyuki Shirase¹, Wen-Hua Lee¹, Yoshihiro Yamada¹, Hiroshi Hiai¹, Junji Yodoi³ and Shinya Toyokuni¹

¹Department of Pathology and Biology of Diseases, Graduate School of Medicine, Kyoto University, Kyoto, Japan; ²Biomedical Special Research Unit, Human Stress Signal Center, National Institute of Advanced Industrial Science and Technology (AIST), Ikeda, Osaka, Japan and ³Department of Biological Responses, Institute for Virus Research, Kyoto University, Kyoto, Japan

Thioredoxin is a major component of thiol-reducing system. Recently, we identified thioredoxin-binding protein-2 (TBP-2) as a negative regulator of thioredoxin. Here, we report the role of TBP-2 in oxidative renal tubular injury and the subsequent carcinogenesis by ferric nitrilotriacetate. TBP-2 was abundantly expressed in the rat kidney. Immunohistochemical analysis revealed that TBP-2 was present in association with nuclei and mitochondrial intermembrane space in the proximal tubular cells and coimmunoprecipitated with cytochrome *c*. After acute oxidative tubular damage, TBP-2 protein, but not messenger RNA, markedly decreased, demonstrating shortened half-life of this protein. Most cases of the induced renal cell carcinoma showed undetectable levels of TBP-2 protein, which was associated with the methylation of CpG island in the promoter region. Genome sequence analyses identified the poly-A tract in the 3' untranslated region as a mutation hot spot in this rather nonselective environment. Collectively, the amounts of TBP-2 protein were inversely associated with proliferation of tubular cells, as evaluated by proliferating cell nuclear antigen. These results suggest that loss of TBP-2 is essential for proliferation of not only neoplastic but also non-neoplastic renal tubular cells, and that TBP-2 is a target gene in oxidative stress-induced renal carcinogenesis by ferric nitrilotriacetate.

Laboratory Investigation (2005) 85, 798–807, advance online publication, 18 April 2005; doi:10.1038/labinvest.3700280

Keywords: oxidative stress; carcinogenesis; kidney; thioredoxin binding protein-2; methylation of CpG island; PCNA; vitamin D; mitochondria

Oxidative stress is intimately associated with carcinogenesis.¹ Iron is the most abundantly present transition metal in the human body, and iron overload has been shown to be associated with carcinogenesis² presumably via its catalytic effect on the generation of reactive oxygen species (ROS).³ However, its precise molecular mechanism still remains unclear.

Administration of an iron chelate, ferric nitrilotriacetate (Fe-NTA), provides an intriguing model of iron-mediated oxidative stress-induced carcino-

genesis: its intraperitoneal administration induces renal proximal tubular damage (as a consequence of the Fenton reaction) that ultimately leads to up to 90% incidence of renal cell carcinoma (RCC) in rodents.^{4–6} This model is characterized by (1) high incidence of pulmonary metastasis and peritoneal invasion, (2) increase in molecules covalently modified by ROS⁷ in the kidney during carcinogenesis, and (3) inhibition of not only acute renal tubular damage but also tumor incidence⁸ by pretreatment with a lipophilic antioxidant, α -tocopherol. We previously reported an increase in a variety of oxidatively modified molecules such as 8-oxoguanine,^{9,10} thymine–tyrosine crosslinks,¹¹ saturated and unsaturated mutagenic aldehydes including 4-hydroxy-2-nonenal (HNE) and malondialdehyde (MDA), and HNE- and MDA-modified proteins^{12–14} in the kidney after Fe-NTA administration. Recently, we identified the *p15^{INK4B}* and

Correspondence: Professor S Toyokuni, MD, PhD, Department of Pathology and Biology of Diseases, Graduate School of Medicine, Kyoto University, Yoshida-Konoe-cho, Sakyo-ku, Kyoto 606-8501, Japan.

E-mail: toyokuni@path1.med.kyoto-u.ac.jp

Received 16 January 2005; revised and accepted 4 March 2005; published online 18 April 2005

p16^{INK4A} tumor suppressor genes^{15,16} and the annexin 2 gene¹⁷ as target genes in this model.

Thioredoxin (Trx) is a 12-kDa ubiquitous protein that has disulfide-reducing activity within its consensus sequence (-Trp-Cys-Gly-Pro-Cys-) and is involved in a variety of cellular functions including proliferation, antiapoptosis and the activation of transcription factors.^{18–20} Trx constitutes one of the major reducing systems in the cell together with Trx reductase and nicotinamide adenine dinucleotide phosphate, reduced form (NADPH).^{21,22}

In 1999, we identified a Trx-binding protein with a yeast two-hybrid assay and named it Trx-binding protein-2 (TBP-2);²³ it was recognized that TBP-2 is identical to vitamin D₃ upregulated protein-1 (VDUP-1)²⁴ or thioredoxin-interacting protein.²⁵ In a more recent work, we found that loss of TBP-2 plays an important role in human T-cell leukemia virus type I-induced T-cell transformation.²⁶ In the present study, we examined the significance of TBP-2 in the Fe-NTA-induced renal cancer model of rats. TBP-2 was abundantly present in the rat renal proximal tubular cells. We report here for the first time that loss or decrease of TBP-2 was a common and critical process for renal tubular proliferation whether it was regenerative or neoplastic, and that TBP-2 was a possible major target gene in this oxidative stress-induced renal carcinogenesis.

Materials and methods

Chemicals

Ferric nitrate enneahydrate, β -nicotinamide adenine dinucleotide phosphate (reduced form), cytochrome *c*, sodium pyruvate and sodium succinate were from Wako (Osaka, Japan); nitrilotriacetic acid disodium salt was from Nacalai Tesque Inc. (Kyoto, Japan). 2-(*p*-Iodophenyl)-3-(*p*-nitrophenyl)-5-phenyltetrazolium chloride and β -nicotinamide adenine dinucleotide (reduced form) were from Sigma (St Louis, MO, USA). All the chemicals used were of analytical quality; deionized water was used throughout. Fe-NTA solution was prepared immediately before use as previously described.¹²

Animal Studies

Fe-NTA-induced RCCs were produced according to a previously described protocol.²⁷ The acute study of a single injection (15 mg iron/kg; 0, 1, 3, 6, 12, 24 and 48 h) and the subacute study of repeated injections (5–10 mg iron/kg; 3 weeks) were carried out as previously described using 5-week-old specific pathogen-free male Wistar rats (Shizuoka Laboratory Animal Center, Shizuoka, Japan).⁹ Fischer-344 and Brown-Norway rat strains were obtained from Charles River Japan Inc. (Yokohama, Japan). The animals were killed and RCCs were collected 12–15 months after the completion of

Fe-NTA administration as described.²⁷ Tumorous and nontumorous portions of renal tissues were excised and stored frozen at -80°C . A total of 22 cases of RCCs (one grade-1 tumor, eight grade-2 tumors and 12 grade-3 tumors, of which 13 showed pulmonary metastasis and six showed peritoneal invasion after classification as described²⁷) and one case of adenoma were used.

Antibodies

Yat315 and Yat818 mouse monoclonal antibodies (IgG₁) were raised against full-length human recombinant TBP-2. These antibodies recognized rat TBP-2.²⁶ Anti-mouse Trx rabbit polyclonal antibody that also recognizes rat Trx was used as described.²⁸ Mouse monoclonal antibody against cytochrome *c* (clone A-8) was obtained from Santa Cruz Biotechnology (Santa Cruz, CA, USA). Monoclonal antibody against proliferating cell nuclear antigen (PCNA; clone PC-10) was from Dako (Kyoto, Japan). Anti-actin monoclonal antibody (clone MAB1501) was purchased from Chemicon International Inc. (Temecula, CA, USA). Horseradish peroxidase-conjugated rabbit antibody against mouse IgG was from Amersham Pharmacia Biotech (Tokyo, Japan), and biotin-labeled rabbit antibody against mouse IgG was from Dako.

Immunoprecipitation and Western Blot Analysis

Tissue lysates were prepared by homogenization in RIPA buffer (20 mM Tris, 0.1% SDS, 1% Triton X-100, 1% sodium deoxycholate, pH 7.4) in the presence of protease inhibitors (complete mini, Roche), and the supernatants collected after centrifugation at 15 000 *g* for 15 min were used. For cellular fractionation, tissues were homogenized in 0.25 M sucrose solution using five strokes of a Potter-type homogenizer, and differential centrifugation was performed. The precipitate after 600 *g* centrifugation for 10 min was regarded as the nuclear fraction; the precipitate after 8000 *g* centrifugation for 10 min was regarded as the mitochondrial fraction; the precipitate after 105 000 *g* for 60 min was regarded as the microsomal fraction; and the remaining supernatant was regarded as the cytosol. The protein concentration was determined with BCA protein reagents (Pierce, Rockford, IL, USA). Biochemical analyses were performed to ascertain the purity of each fraction. High amount of DNA content was considered as an indicator for the nuclear fraction.²⁹ Succinate dehydrogenase activity as an indicator for the mitochondrial fraction was determined by estimating the reduction of 2-(*p*-iodophenyl)-(p-nitrophenyl)-5-phenyl tetrazolium chloride.³⁰ NADPH-cytochrome *c* reductase activity as an indicator of the microsomal fraction was determined by measuring the reduction of cytochrome *c* at 550 nm. The reaction was

conducted at 30°C in a high ionic strength buffer as described.^{31,32} Lactate dehydrogenase (LDH) activity as an indicator of cytosolic fraction was determined by estimating the consumption of β -nicotinamide adenine dinucleotide (NADH) and the progression was observed at 340 nm.³³

Immunoprecipitation was performed as described¹⁷ using 10 μ l of Yat315 monoclonal antibody added to 400 μ g of lysate in a 100- μ l volume. IgG₁ immunoglobulin (Dako, clone DAK-GO1) was used as a negative control. The Sepharose beads were separated by centrifugation, and boiled with 50 μ l of sample buffer containing 2-mercaptoethanol for 3 min. In all, 20 μ l of the supernatant was electrophoresed in each lane for sodium dodecyl sulfate-polyacrylamide gel electrophoresis (SDS-PAGE). Western blotting was carried out as previously described.³⁴ NIH image freeware (ver. 1.62, <http://rsb.info.nih.gov/nih-image/>) was used for the densitometric analyses.

Immunohistochemical Analysis

Tissues were fixed with 10% neutral formalin overnight, embedded in paraffin, cut at 3- μ m thickness, and used for hematoxylin and eosin staining or immunohistochemistry. The avidin-biotin complex method with peroxidase was used for immunohistochemistry as described.¹⁰ Antigen retrieval with a standard microwave irradiation method in 10 mM citrate buffer, pH 7.4, was used. For electronmicroscopic analyses, a pre-embedding method was used. Briefly, paraffin-embedded specimens were cut at 8- μ m thickness, and immunohistochemistry was performed as described above. 3,3'-Diaminobenzidine solution (Dako Liquid DAB, K3466) was used for color development. Thereafter, the specimens were immediately postfixed with 2% glutaraldehyde in 50 mM phosphate-buffered saline, pH 7.4, for 45 min, dehydrated in a graded ethanol series, and embedded in Epon 812. Sections were cut with a diamond knife on a Sorvall MT-5000 ultramicrotome, mounted on copper grids coated with polyvinylformal, left unstained or stained with uranyl acetate, and observed with a Hitachi HU-12A electronmicroscope.

Northern Blot Analysis

Total RNA was isolated by means of a modified acid guanidinium phenol chloroform method (Isogen, Nippon Gene, Tokyo). Poly(A)-rich RNA was isolated using oligo(dT)-latex beads (Nippon Roche, Tokyo). For Northern blot analysis, poly(A)-rich RNA samples (2 μ g) were separated by electrophoresis on a 1% agarose gel containing formaldehyde and transferred onto a nylon membrane. DNA fragments of rat TBP-2 (GenBank XM 215640: 510-1494) were amplified by PCR (sense, 5'-CCTACAGGTGAGAACCAGATGGTG-3'; antisense,

5'-GGCAGAAAGCGTTGAGTAGTAGTACAGAT-3') using rat kidney cDNA as a substrate, purified and used as a probe after labeling with [α -³²P]dCTP by the random priming method (Megaprime DNA labeling kit, Amersham Pharmacia Biotech). Hybridization was performed as previously described.¹⁷

Mutational Analysis

Genomic sequences of TBP-2 were amplified using seven different sets (forward, F; reverse, R) of primers: F1 5'(-1035)GTGGACACTCCCTTACTGCTTCCGT(-1011)-3' and R1 5'(-355)CTCGTGCACAGTTCTCCCATTTGGCT(-379)-3' (681 base pairs (bp); base numbers calculated from the first ATG codon); F2 5'(-396)GTAAACAAGGACCAAGTAGCCAATG(-372)-3' and R2 5'(+237)TTCTAGGAGAAGGGTGTCTTCATAG(+213)-3' (633 bp); F3 5'(+465)AAGATTAATGTATTCGTGGGTTGTG(+489)-3' and R3 5'-(+1120)GAACATGCAGGAACTTTCTTCTC(+1097)-3' (656 bp); F4 5'-(+949)ACTCCTGACTTAA TGTTGAGGCTT(+972)-3' and R4 5'-(+1651)AGG TGGGAGTTTGTAGATGGGTT(+1628)-3' (703 bp); F5 5'-(+1547)AGAGTTGAATACTCCTTGCTGGTGA(+1571)-3' and R5 5'-(+2314)TCTGAAACATTGGA GTTCAAGCAGA(+2290)-3' (768 bp); F6 5'-(+2168)AAATCTGAAAGTCTCCTCGCTCTTC(+2192)-3' and R6 5'-(+2938)GCTAAAGTGCCAAGAACATCACCT(+2915)3' (771 bp); F7 5'-(+2905)ATTGATTCTAA GGTGATGTTCTTGG(+2929)-3' and R7 5'-(+3696)GGCAGAGGAAAACCTGAAGATACCTA(+3672)-3' (792 bp). These amplified sequences covered all the exon sequences and more than 80% of the intronic sequences (~95% of the total TBP-2 gene area). PCR was performed in a 12.5- μ l reaction mixture. The mixture contained 1 \times PfuUltra high fidelity (HF) reaction buffer (Stratagene, La Jolla, CA, USA), dNTPs (0.3 mM each) (Takara, Shiga, Japan), primers (5 pmol per reaction mixture), template DNA (30 ng) and 0.63 unit of PfuUltra HF DNA Polymerase (Stratagene, La Jolla, CA, USA). Amplification was carried out for 35 cycles (30 s at 95°C, 30 s at 58°C and 75 s at 72°C), followed by a final 10-min extension at 72°C. A zero blunt TOPO cloning kit (Invitrogen, Carlsbad, CA, USA) was used according to the manufacturer's instructions. Sequencing was performed using chain terminating big dye (Applied Biosystems, Foster city, CA, USA) and the sequences were compared with the rat genome database (NCBI, <http://www.ncbi.nlm.nih.gov/>) to evaluate the mutations.

Methylation-Specific PCR

Genomic DNA was extracted as described,³⁵ and methylation-specific PCR was performed as described.³⁶ The primers used are summarized in Table 1.

Table 1 Primer pairs for methylation-specific PCR

Primer set	Sense and antisense primers	Product Size (bp)	Annealing temperature (°C)
Methylated (Modified DNA)	S:5'(-423)CGGTTTCGTTGATTGGTTAGAGGTTT(-398)3' A:5'(-309)TAACTTAACGCTCCACGCG(-327)3'	115	64
Unmethylated (Modified DNA)	S:5'(-421)GTTTTGTTGATTGGTTAGAGGTTTGGTAAAT(-391)3' A:5'(-302)AACCACCTAACTTAACACTCCACACAAATACTA(-334)3'	120	68
Control (Unmodified DNA)	S:5'(-393)AACAAGGACCAAGTAGCCAATG(-372)3' A:5'(-271)TGTC AAGCGGGAGCCGAAA(-290)3'	123	65

S, sense; A, antisense; bp, base pairs.

Results

TBP-2 and Trx Protein Analysis

In this model, acute renal tubular necrosis is observed 3 h after an intraperitoneal administration of Fe-NTA (15 mg iron/kg). Necrosis is prominent at 24 h, but tubular regeneration supervenes at 48 h. After repeated administration of Fe-NTA for 3 weeks, little necrosis is observed but karyomegalic cells appear.⁹

TBP-2 was most abundant in the untreated rat kidney among the tissues examined by Western blot analysis (Figure 1a). However, the amount was significantly decreased to less than 10% of the original amount 12–48 h after Fe-NTA administration. After the repeated administration of Fe-NTA for 3 weeks, a significant decrease of the amount of TBP-2 was observed. Furthermore, 21 out of 22 RCCs (95.5%) showed an undetectable amount of TBP-2. One adenoma (data not shown) and 1 RCC showed decreased amounts of TBP-2 (Figure 1b). The pattern of Trx protein expression was different from that of TBP-2 in that Trx protein was increased at 48 h, and that RCCs showed different levels of Trx protein according to their malignant potential. Basically, high-grade carcinoma expressed higher amounts of Trx (Figure 1b).

TBP-2 mRNA Analysis

Notably, TBP-2 message remained at an almost constant level after oxidative renal tubular injury by Fe-NTA, and increased at 48 h. RCCs showed significantly decreased levels of TBP-2 message (Figure 1c).

Immunohistochemical Analysis

By immunohistochemical analyses, TBP-2 was detected in the cytoplasm and nuclei of the renal proximal tubular cells, but not in the glomeruli. The cytoplasm showed a distinct granular pattern (Figure 2a). After oxidative tubular damage, the survived tubular cells lost the immunostaining (data not shown). After 3 weeks of Fe-NTA treatment, some renal proximal cells showed immunostaining,

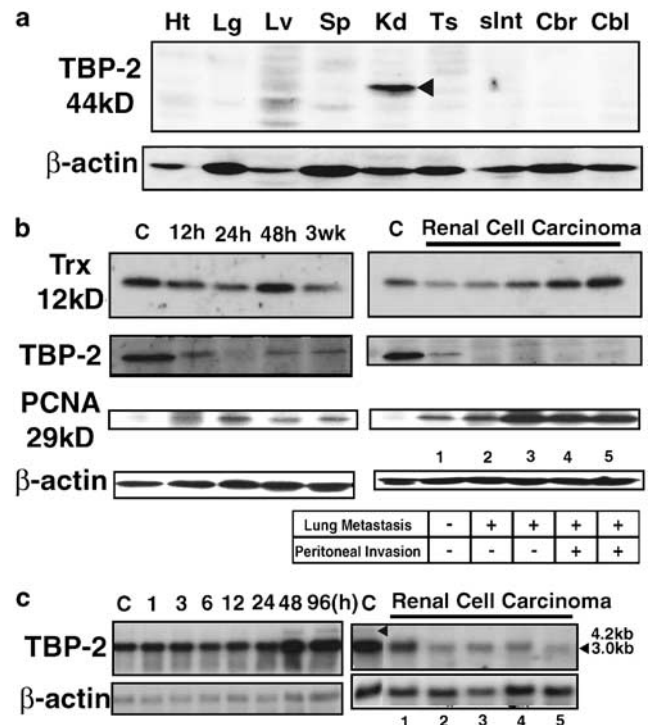


Figure 1 Characterization of TBP-2 expression in rat normal organs, kidney after Fe-NTA administration and Fe-NTA-induced renal cell carcinoma. (a) The highest level of thioredoxin-binding protein-2 (TBP-2) was detected by Western blot analysis in the kidney (arrowhead). Ht, heart; Lg, lung; Lv, liver; Sp, spleen; Kd, kidney; Ts, testis; sInt, small intestine; Cbr, cerebellum; Cbl, cerebellum. (b) Western blot analysis of thioredoxin (Trx), TBP-2 and proliferating cell nuclear antigen (PCNA). Decrease or loss of TBP-2 protein in the kidney was observed after an administration of ferric nitrilotriacetate (Fe-NTA; 12, 24 and 48 h) or after repeated administration (3 weeks). Loss of TBP-2 was observed in most of the Fe-NTA-induced renal cell carcinomas (RCCs). Decrease or loss of TBP-2 was associated with increase in PCNA (refer to Figure 4). The Trx protein level was basically proportional with the malignant behavior of the tumor. C, untreated control kidney. See text for details. (c) Northern blot analysis of TBP-2 and β -actin. The levels of TBP-2 message (lower arrowhead) remained almost unchanged or were rather increased after an administration of Fe-NTA (1, 3, 6, 12, 24, 48 and 96 h), whereas that in the RCCs was significantly decreased. The samples of RCCs in (b) and (c) correspond each other (1–5). A minor band of 4.2 kb was observed (upper arrowhead).

but other cells including karyomegalic cells showed no staining (Figure 2e). RCCs showed undetectable levels of immunostaining (Figure 2f).

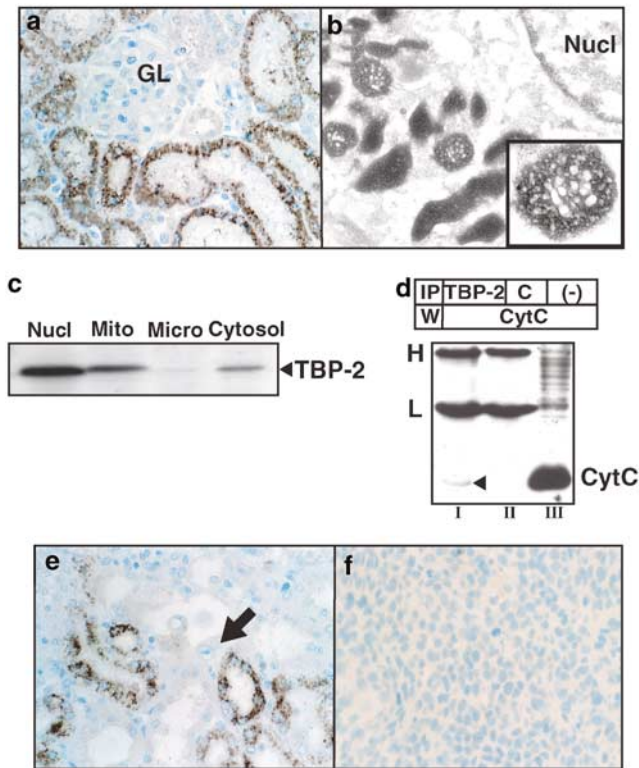


Figure 2 Immunohistochemical analysis of TBP-2. (a) Immunohistochemical analysis of rat untreated control kidney. Granular positivity was observed in the proximal tubular cells. GL, glomerulus (original magnification, $\times 200$). (b) Electronmicroscopic immunohistochemical analysis of rat control kidney. Inset shows magnified view of a mitochondrion. Mitochondrial intermembrane space and nucleus show electron-dense positivity. Nucl, nucleus (original magnification, $\times 7000$). (c) Western blot analysis of rat control kidney after fractionation. Nucl, nuclear fraction; Mito, mitochondrial fraction; Micro, microsomal fraction. See text for details. (d) Immunoprecipitation analysis showing the association of TBP-2 and cytochrome *c*. IP, immunoprecipitation; W, western blot analysis; C, negative control IgG₁ immunoglobulin; CytC, cytochrome *c*; H, immunoglobulin heavy chain; L, immunoglobulin light chain. Mitochondrial fraction (1 μ g) was run as a control in lane III. (e) Immunohistochemical analysis of a kidney 3 weeks after repeated administration of Fe-NTA. A karyomegalic cell (arrow) was negative for TBP-2. (f) Immunohistochemical analysis of Fe-NTA-induced RCC. Tumor cells were negative (original magnification, $\times 200$).

Subcellular Localization of TBP-2

This study was performed on the untreated control kidney. Fractionation was performed by differential centrifugation to nuclear, mitochondrial, microsomal and cytosolic fractions, followed by confirmation with biochemical markers: DNA content, 196, 5.8, 0.0 and 2.4 μ g/mg protein, respectively; succinate dehydrogenase activity, 0.0, 800, 0.0 and 0.0 OD at 490 nm/min/mg protein, respectively; NADPH-cytochrome *c* reductase activity, 0.050, not applicable, 83.0 and 0.013 nmol/min/ μ g protein, respectively; LDH activity, 16, 5.0, 14 and 100 mU/mg protein, respectively. Western blot analysis revealed that major amounts of TBP-2 were

present in the nuclei and mitochondria, a small amount in the cytosol, and almost none in the microsomal fraction (Figure 2c). Immunohistochemistry at the electronmicroscopic level showed the presence of TBP-2 in the intermembrane space of mitochondria and nuclei (Figure 2b). Immunoprecipitation analyses of the mitochondrial fraction revealed the association of TBP-2 with cytochrome *c* (Figure 2d).

Mutational Analysis of TBP-2

Rat TBP-2 genome sequences were obtained from the NCBI rat genome database. This gene was located on chromosome 2, and spanned 3875 bp with eight exons. Positions -785 to -208 from the initiation ATG codon were categorized as a CpG island with a CpG island searcher program (<http://ccnt.hsc.usc.edu/cpgislands/>) (Figure 3a). We found a unique type of deletion polymorphism in this CpG island producing interstrain differences at a potential site for methylation (Figure 3b and c). The poly-A tract in the distal part of the 3' untranslated region (UTR) also showed some variation of the number of mononucleotide repeats in different strains of rats. In the Wistar and Fischer-344 strains, the number of repeats was 16, whereas it was 15 in the Brown-Norway strain. Furthermore, the poly-A tract in the 3' UTR was a frequent site for insertion and deletion mutations in the RCCs. The incidence of mutations was much lower in the coding exons and introns, and the mutations were all apparently silent (Table 2).

CpG Island Methylation in the RCCs

Methylation-specific PCR analysis revealed that all the tumors examined showed methylation at the examined position of CpG island in the promoter region of TBP-2 gene (Figure 3d).

Association between TBP-2 and Cellular Proliferation

Immunohistochemical analyses by the use of serial paraffin-embedded sections as well as Western blot analyses showed that PCNA positivity and TBP-2 positivity were inversely associated (Figures 1 and 4a–d). After quantitating the results, the amounts of TBP-2 protein were significantly and inversely associated with the fraction of PCNA-positive cells with a certain threshold (Figure 4e). In the present study, TBP-2 protein was undetectable by Western blot analysis when the fraction of PCNA-positive cells in the tissue was approximately more than 55%. Within the range of 3–55% of PCNA-positive cell fraction, the correlation coefficient was $r^2 = 0.988$ ($P < 0.01$).

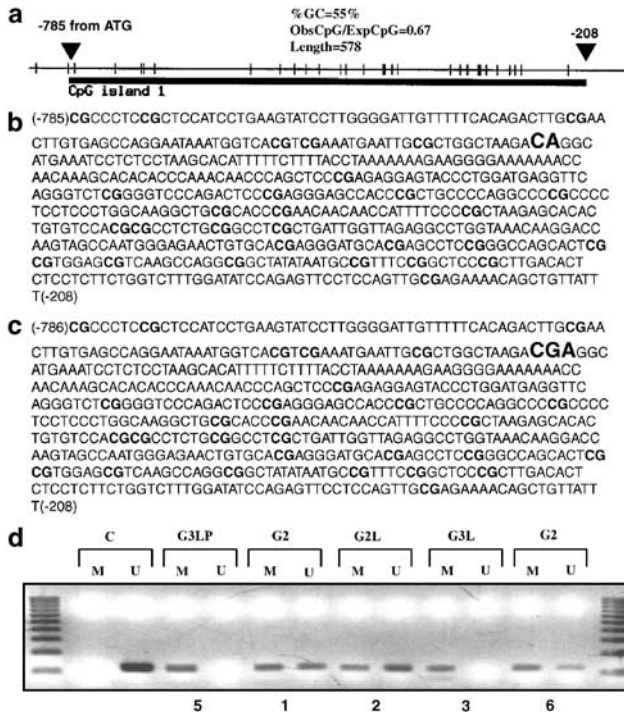


Figure 3 Genome structure and methylation-specific PCR analysis of rat TBP-2. (a) Structure of CpG island in the promoter region. (b) CpG island in the Brown-Norway strain. (c) CpG island in the Fischer-344 and Wistar strains. (d) Methylation-specific PCR analysis of TBP-2. All the tumors examined showed methylation at the CpG site amplified with the primer pairs shown in Table 2. Sample numbers shown at the bottom of Figure 3d correspond with those of Figure 1 and Table 2. M, methylated; U, unmethylated; C, untreated control kidney; G2, grade-2; G3, grade-3; L, lung metastasis; P, peritoneal invasion.

Discussion

We found that the TBP-2 gene is one of the major target genes in Fe-NTA-induced renal carcinogenesis. The mode of inactivation was transcriptional silencing via CpG island methylation, as previously observed in one-third of the cases of inactivation of *p15^{INK4B}* and *p16^{INK4A}* tumor suppressor genes in this model.¹⁵ Furthermore, loss of TBP-2 in human T-cell leukemia virus I-transformed cell lines was associated with aberrant methylation of CpG island region (Ahsan KM, Masutani H and Yodoi J, unpublished data). This suggests the presence of certain common mechanisms facilitating the methylation of CpG island regions during oxidative stress-induced carcinogenesis that should be further explored.

We also observed interstrain polymorphisms and several kinds of mutations (Figure 3b, c and Table 1). All the mutations were apparently silent. However, in this rather nonselective genomic environment we may be able to evaluate the unbiased spectrum of ROS-induced mutagenesis. We found a high incidence of single nucleotide insertions or deletions in the poly-A tract of the

distal part of 3' UTR. The C:G to T:A transition and G:C to T:A transversion mutations observed can be explained by the ROS-induced DNA base modifications.³

Furthermore, we found that a decrease in TBP-2 was associated with non-neoplastic cellular proliferation *in vivo*, namely, the regeneration of renal proximal tubules (Figure 1b). In this situation, however, ample amounts of message were observed (Figure 1c), suggesting that certain post-transcriptional mechanisms play a role in shortening the half-life of this protein. One of the plausible explanations is that certain organelles work as a temporary reservoir for TBP-2. This will be discussed later in detail. We then studied the relationship between cellular proliferation and the presence of TBP-2 protein, and found that a decrease in TBP-2 was closely associated with the presence of PCNA (Figures 1b and 4e). This was further confirmed by a morphological study revealing that TBP-2-positive cells were negative for PCNA and *vice versa* (Figure 4a–d).

To elucidate the biological significance of the above observations, we examined the precise intracellular localization of TBP-2 in the rat kidney. The ubiquity of TBP-2 mRNA has been reported. However, we found an organ-specific difference in the amounts of TBP-2 protein (Figure 1a). We believe that this is due to the fact that most of the previous studies assessed only TBP-2 mRNA, not protein. Studies showed increased levels of TBP-2 mRNA after oxidative stress³⁷ or glucose loading,³⁸ and a decrease in the mRNA level in several human^{39–41} and animal tumors.⁴² Re-evaluation of these experiments may be necessary because of the inconsistency between the mRNA and protein levels of TBP-2.

Our fractionation study revealed that TBP-2 was present mainly in the nuclear and mitochondrial fractions in the renal proximal tubules (Figure 2c), which was consistent with the observation with immunostaining (Figure 2a). Immunohistochemical analysis at the electronmicroscopic level clearly showed that TBP-2 was present in the intermembrane space of mitochondria (Figure 2b) and in the nucleus. Cytochrome *c* is a soluble protein that associates through electrostatic interactions with the outer surface of the mitochondrial inner membrane and is involved in complexes III and IV in the oxidative phosphorylation, and its release to the cytoplasm is one of the signals for the start of apoptosis.⁴³ In our immunoprecipitation study, we unexpectedly found that TBP-2 was associated with cytochrome *c* (Figure 2d). Although the fraction of cytochrome *c* bound to TBP-2 appears small, this confirms the presence of TBP-2 in the intermembrane space of the mitochondria.

Protein interaction of TBP-2 in mitochondria merits immediate attention. It is well known that renal proximal tubular cells are metabolically active and are rich in mitochondria.⁴⁴ The precise role of

Table 2 Mutational spectrum of the TBP-2 gene in Fe-NTA-induced renal cell tumors

Tumor sample ID	Strain details	Features of the tumors				Mutational change	Location of the mutation
		Lung metastasis	Peritoneal invasion	Size (mm)	Histology and grading		
16-5 ^a	W	–	–	10	Adenoma	Single nucleotide (A) insertion	A ₁₆ tract in the distal part of 3' UTR (+3571 → +3586)
2-1	W	+	+	90	RCC grade 2	Single nucleotide (A) insertion C → T	A ₁₆ tract in the distal part of 3' UTR (+3571 → +3586) Promoter (–311)
7-1 ^a (1) ^b	F1(F × BN)	–	–	20	RCC grade 2	A → T	Coding sequence, synonymous (+1081)
7-7 (2)	F1(F × BN)	+	–	60	RCC grade 2	–	–
14-1	W	+	–	17	RCC grade 2	G → T Single nucleotide (A) insertion	3' UTR (+3158) A ₁₆ tract in the distal part of 3' UTR (+3571 → +3586)
15-3(6)	W	–	–	50	RCC grade 2	–	–
48-5	F1(F × BN)	–	–	20	RCC grade 2	–	–
14-6(5)	F1(F × BN)	+	+	30	RCC grade 3	Single codon (AAC) deletion Single nucleotide deletion (A)	Coding sequence, carboxy-terminal Asn ₆ tract (+2218 → +2235) A ₁₅ tract in the distal part of 3' UTR (+3571+3586)
15-4	W	+	+	40	RCC grade 3	G → A Single nucleotide deletion (A)	Intronic sequence (+1223) A ₇ in the CpG island (–616 → –622),
16-1	W	+	–	40	RCC grade 3	Single nucleotide (A) insertion	A ₁₆ tract in the distal part of 3' UTR (+3571+3586)
30-5(4)	F1(F × BN)	+	+	60	RCC grade 3	–	–
45-4(3)	F1(F × BN)	+	–	40	RCC grade 3	–	–

RCC, renal cell carcinoma; W, Wistar strain; F, Fischer strain; BN, Brown-Norway strain; UTR, untranslated region.

^aShowed small amount of TBP-2 protein by Western blot analysis. TBP-2 protein was undetectable in all the other tumors.

^bNumbers in the parentheses after tumor sample ID correspond to the tumor numbers in Figures 1b and 3d. Refer to text for details.

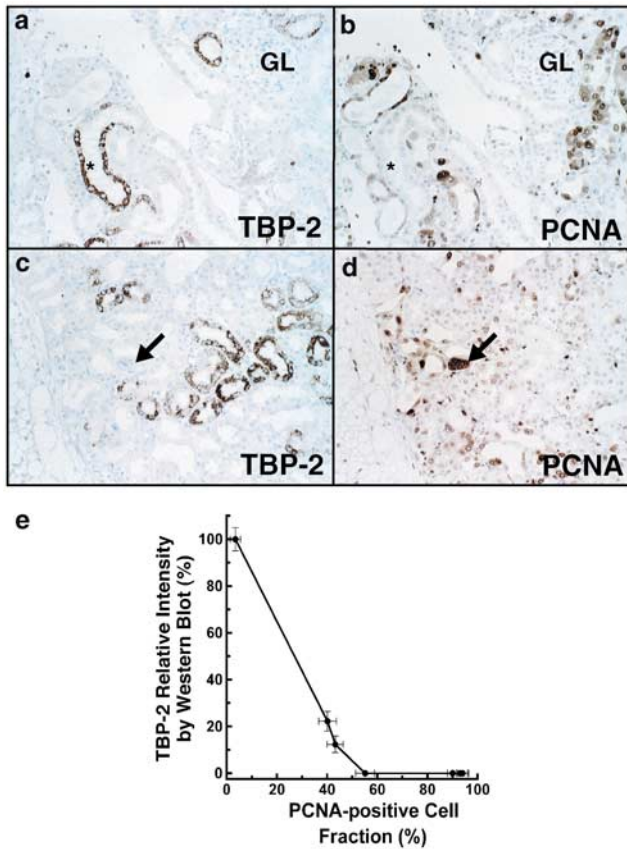


Figure 4 Inverse association of TBP-2 and cellular proliferation *in vivo*. (a) and (c) Immunohistochemical analysis of TBP-2 in the kidney after repeated Fe-NTA administration of 3 weeks. (b) and (d) Immunohistochemical analysis of PCNA in the kidney after the same repeated Fe-NTA administration (original magnification, $\times 200$). (a and b), (c and d) are paired serial sections, and asterisks and arrows show identical positions. TBP-2-positive cells and PCNA-positive cells were complementary to each other. (e) Inverse association between PCNA-positive cell fraction and amounts of TBP-2 protein. The amount of TBP-2 by Western blot analysis was quantified with NIH image freeware as described in the Materials and methods section. PCNA-positive cell fraction was determined by counting positive cells at five randomly selected areas ($\times 200$ magnification). Three samples of renal tissues were used for each point (control, 24 h, 48 h, 3 weeks, RCCs; $N = 3$, means \pm s.e.m.). Within the range of 3–55% of PCNA-positive cell fraction, an inverse correlation was observed between the amount of TBP-2 protein and cellular proliferation. Refer to text for details.

TBP-2 in the renal proximal tubules is unknown so far, but there are possible functions from at least three standpoints.

First, TBP-2 was reported as VDUP-1 in HL-60 leukemia cells.²⁴ HL-60 cells differentiate into monocytes or macrophages on exposure to vitamin D₃.⁴⁵ Vitamin D is a seco-steroid whose actions are dependent on several steps catalyzed by cytochrome P450 enzymes. The first of these steps is carried out in the liver by the enzyme 25-hydroxylase, which catalyzes the synthesis of 25-hydroxyvitamin D₃ (25(OH)D₃), the major circulating form of vitamin D₃. The 25(OH)D₃ is then converted to the active

form of vitamin D, dihydroxyvitamin D₃, by the enzyme 25-hydroxyvitamin D₃-1 α -hydroxylase present in the mitochondria of renal proximal tubules.⁴⁶ TBP-2 was indeed accumulated in the location where vitamin D is activated.

Second, TBP-2 is a binding protein of Trx. The ubiquitous enzyme Trx is responsible for equilibrating the NAD(P)H/NAD⁺(P) redox potential together with the protein sulfhydryl redox state via the oxidation of NADPH. We have reported that Trx function can be modulated by the interaction with its inhibitory protein, TBP-2.²³ Recently, studies of a TBP-2-null mutant mouse²⁵ provided evidence that loss of TBP-2 results in enhanced sulfhydryl reduction and dysregulated carbohydrate and lipid metabolism, namely hyperinsulinemia, hypoglycemia, hypertriglyceridemia and increased levels of ketone bodies, at least in the liver and pancreatic β -cells.⁴⁷ On the other hand, it was shown that hyperglycemia inhibits the ROS-scavenging function of Trx through p38 MAPK-induction of TBP-2.⁴⁸ In the present study of renal carcinogenesis, loss of TBP-2 protein was induced only in a certain fraction of the renal tubular cells after Fe-NTA treatment and in the cancer cells (Figure 2e and f). Loss of TBP-2 appears advantageous in cancer cells because it results in facilitation of the glycolytic pathway⁴⁷ in addition to the promotion of cellular proliferation since hypoxia is often associated with tumor growth. In a yeast two-hybrid screening using TBP-2 as bait, several clones encoding Trx2 were identified, demonstrating the interaction of TBP-2 with Trx2 *in vitro* (Wang D, Masutani H and Yodoi J, unpublished data). Studies are in progress to clarify the association among TBP-2, Trx2 and cytochrome *c*.

Third, mitochondria may work as a temporary reservoir for TBP-2. The nucleus appears to be the final destination of this protein. We found that TBP-2 ectopically expressed in the breast cancer cell line MCF-7 was localized predominantly in the nucleus exhibiting growth suppressive activity.⁴⁹ It was also reported that TBP-2 interacts with promyelocytic leukemia zinc-finger, Fanconi anemia zinc-finger and histone deacetylase 1, which are known to be transcriptional corepressors.⁴¹ As a nuclear transport system, we recently identified importin α_1 (Rch1) as a protein interacting with TBP-2. The expression of short interfering RNA of importin α_1 suppressed suberoylanilide hydroxamic acid-induced nuclear accumulation of TBP-2.^{49,50} Renal function is essential for the survival of the individual. A regulatory mechanism to maintain the renal tubular function by inhibiting mitosis may be necessary when a low level of damage occurs in the mitochondria of renal proximal tubules. In the Fe-NTA model, we previously reported that the mitochondria are major target organelles in the acute renal tubular injury by Fe-NTA.⁵¹ It is possible that mild damage to mitochondria induces a release of TBP-2 to nuclei, leading to inhibition of mitosis. Severe damage or loss of

mitochondria may lead to loss of TBP-2 protein, resulting in a signal for mitosis. Renal proximal tubule is a site that merits further investigation of TBP-2 function *in vivo*.

In conclusion, TBP-2 protein is abundant in the mitochondria of the rat renal proximal tubular cells, where vitamin D is converted to an active form, and in the nuclei of these cells. TBP-2 expression is transcriptionally silenced in Fe-NTA-induced RCCs of rats by aberrant promoter methylation. Loss of TBP-2 is intimately associated with renal tubular proliferation *in vivo* irrespective of the molecular mechanisms involved and whether such proliferation is neoplastic or non-neoplastic.

Acknowledgements

We thank Ms Waka Kawaguchi for excellent technical assistance. This work was supported in part by a Grant-in-Aid from the Ministry of Education, Science, Sports and Culture of Japan and a Grant-in-Aid for Cancer Research from the Ministry of Health, Labour and Welfare of Japan. The sequences reported in this paper have been deposited in the DDBJ/EMBL/GenBank database (Accession: AB189076 and AB189077).

References

- Ames BN, Shigenaga MK, Park E-M. DNA damage by endogenous oxidants as a cause of aging and cancer. In: Davies KJA (ed). *Oxidative Damage and Repair: Chemical Biological and Medical Aspects*. Pergamon Press: New York, 1991, pp 181–187.
- Wu T, Sempos C, Freudenheim J, *et al*. Serum iron, copper and zinc concentrations and risk of cancer mortality in US adults. *Ann Epidemiol* 2004;14: 195–201.
- Toyokuni S. Iron-induced carcinogenesis: the role of redox regulation. *Free Radic Biol Med* 1996;20: 553–566.
- Ebina Y, Okada S, Hamazaki S, *et al*. Nephrotoxicity and renal cell carcinoma after use of iron- and aluminum- nitrilotriacetate complexes in rats. *J Natl Cancer Inst* 1986;76:107–113.
- Li JL, Okada S, Hamazaki S, *et al*. Subacute nephrotoxicity and induction of renal cell carcinoma in mice treated with ferric nitrilotriacetate. *Cancer Res* 1987;47:1867–1869.
- Toyokuni S, Okada S, Hamazaki S, *et al*. Combined histochemical and biochemical analysis of sex hormone dependence of ferric nitrilotriacetate-induced renal lipid peroxidation in ddY mice. *Cancer Res* 1990;50:5574–5580.
- Toyokuni S. Reactive oxygen species-induced molecular damage and its application in pathology. *Pathol Int* 1999;49:91–102.
- Zhang D, Okada S, Yu Y, *et al*. Vitamin E inhibits apoptosis, DNA modification, and cancer incidence induced by iron-mediated peroxidation in Wistar rat kidney. *Cancer Res* 1997;57:2410–2414.
- Toyokuni S, Mori T, Dizdaroglu M. DNA base modifications in renal chromatin of Wistar rats treated with a renal carcinogen, ferric nitrilotriacetate. *Int J Cancer* 1994;57:123–128.
- Toyokuni S, Tanaka T, Hattori Y, *et al*. Quantitative immunohistochemical determination of 8-hydroxy-2'-deoxyguanosine by a monoclonal antibody N45.1: its application to ferric nitrilotriacetate-induced renal carcinogenesis model. *Lab Invest* 1997;76:365–374.
- Toyokuni S, Mori T, Hiai H, *et al*. Treatment of Wistar rats with a renal carcinogen, ferric nitrilotriacetate, causes DNA-protein cross-linking between thymine and tyrosine in their renal chromatin. *Int J Cancer* 1995;62:309–313.
- Toyokuni S, Uchida K, Okamoto K, *et al*. Formation of 4-hydroxy-2-nonenal-modified proteins in the renal proximal tubules of rats treated with a renal carcinogen, ferric nitrilotriacetate. *Proc Natl Acad Sci USA* 1994;91:2616–2620.
- Uchida K, Fukuda A, Kawakishi S, *et al*. A renal carcinogen ferric nitrilotriacetate mediates a temporary accumulation of aldehyde-modified proteins within cytosolic compartment of rat kidney. *Arch Biochem Biophys* 1995;317:405–411.
- Toyokuni S, Luo XP, Tanaka T, *et al*. Induction of a wide range of C_{2–12} aldehydes and C_{7–12} acylolins in the kidney of Wistar rats after treatment with a renal carcinogen, ferric nitrilotriacetate. *Free Radic Biol Med* 1997;22:1019–1027.
- Tanaka T, Iwasa Y, Kondo S, *et al*. High incidence of allelic loss on chromosome 5 and inactivation of *p15^{INK4B}* and *p16^{INK4A}* tumor suppressor genes in oxystress-induced renal cell carcinoma of rats. *Oncogene* 1999;18:3793–3797.
- Hiroyasu M, Ozeki M, Kohda H, *et al*. Specific allelic loss of *p16^{INK4A}* tumor suppressor gene after weeks of iron-mediated oxidative damage during rat renal carcinogenesis. *Am J Pathol* 2002;160:419–424.
- Tanaka T, Akatsuka S, Ozeki M, *et al*. Redox regulation of annexin 2 and its implications for oxidative stress-induced renal carcinogenesis and metastasis. *Oncogene* 2004;23:3980–3989.
- Nakamura H, Nakamura K, Yodoi J. Redox regulation of cellular activation. *Annu Rev Immunol* 1997;15: 351–369.
- Nishiyama A, Masutani H, Nakamura H, *et al*. Redox regulation by thioredoxin and thioredoxin-binding proteins. *IUBMB Life* 2001;52:29–33.
- Tanaka T, Nakamura H, Nishiyama A, *et al*. Redox regulation by thioredoxin superfamily; protection against oxidative stress and aging. *Free Radic Res* 2001;33:851–855.
- Holmgren A. Thioredoxin. *Annu Rev Biochem* 1985; 54:231–237.
- Haendeler J, Hoffmann J, Tischler V, *et al*. Redox regulatory and anti-apoptotic functions of thioredoxin depend on S-nitrosylation at cysteine 69. *Nat Cell Biol* 2002;4:743–749.
- Nishiyama A, Matsui M, Iwata S, *et al*. Identification of thioredoxin-binding protein-2/vitamin D₃ up-regulated protein 1 as a negative regulator of thioredoxin function and expression. *J Biol Chem* 1999;274:21645–21650.
- Chen K, De Luca H. Isolation and characterization of a novel cDNA from HL-60 cells treated with 1,25-dihydroxyvitamin D-3. *Biochim Biophys Acta* 1994;1219:26–32.

- 25 Bodnar J, Chatterjee A, Castellani L, *et al*. Positional cloning of the combined hyperlipidemia gene Hyplip1. *Nat Genet* 2002;30:110–116.
- 26 Nishinaka Y, Nishiyama A, Masutani H, *et al*. Loss of thioredoxin-binding protein-2/vitamin D3 up-regulated protein 1 in human T-cell leukemia virus type I-dependent T-cell transformation: implications for adult T-cell leukemia leukemogenesis. *Cancer Res* 2004;64:1287–1292.
- 27 Nishiyama Y, Suwa H, Okamoto K, *et al*. Low incidence of point mutations in H-, K- and N-ras oncogenes and p53 tumor suppressor gene in renal cell carcinoma and peritoneal mesothelioma of Wistar rats induced by ferric nitrilotriacetate. *Jpn J Cancer Res* 1995;86:1150–1158.
- 28 Tanaka T, Nishiyama Y, Okada K, *et al*. Induction and nuclear translocation of thioredoxin by oxidative damage in the mouse kidney: independence of tubular necrosis and sulfhydryl depletion. *Lab Invest* 1997;77:145–155.
- 29 Seol K, Kim S. Nuclear matrix association of insulin receptor and IRS-1 by insulin in osteoblast-like UMR-106 cells. *Biochem Biophys Res Commun* 2003;306:898–904.
- 30 Yamaguchi M, Tsurusaki Y, Misawa H, *et al*. Potential role of regucalcin as a specific biochemical marker of chronic liver injury with carbon tetrachloride administration in rats. *Mol Cell Biochem* 2002;241:61–67.
- 31 Phillips AH, Langdon RG. Hepatic triphosphopyridine nucleotide-cytochrome c reductase: isolation, characterization and kinetic studies. *J Biol Chem* 1962;237:2652–2660.
- 32 Vermilion J, Coon M. Purified liver microsomal NADPH-cytochrome P-450 reductase. Spectral characterization of oxidation-reduction states. *J Biol Chem* 1978;253:2694–2704.
- 33 Kaplan LA, Pesce AJ. *Clinical Chemistry, Theory, Analysis and Correlation*. Mosby: St Louis, 1989.
- 34 Toyokuni S, Kawaguchi W, Akatsuka S, *et al*. Inter-mittent microwave irradiation facilitates antigen-antibody reaction in Western blot analysis. *Pathol Int* 2003;53:259–261.
- 35 Sambrook J, Fritsch EF, Maniatis T. *Molecular Cloning: A Laboratory Manual*. Cold Spring Harbor Laboratory Press: Cold Spring Harbor, NY, 1989.
- 36 Herman JG, Graff JR, Myohanen S, *et al*. Methylation-specific PCR: a novel PCR assay for methylation status of CpG islands. *Proc Natl Acad Sci USA* 1996;93:9821–9826.
- 37 Junn E, Han S, Im J, *et al*. Vitamin D3 up-regulated protein 1 mediates oxidative stress via suppressing the thioredoxin function. *J Immunol* 2000;164:6287–6295.
- 38 Hirota T, Okano T, Kokame K, *et al*. Glucose down-regulates Per1 and Per2 mRNA levels and induces circadian gene expression in cultured Rat-1 fibroblasts. *J Biol Chem* 2002;277:44244–44251.
- 39 Ikarashi M, Takahashi Y, Ishii Y, *et al*. Vitamin D3 up-regulated protein 1 (VDUP1) expression in gastrointestinal cancer and its relation to stage of disease. *Anticancer Res* 2002;22:4045–4048.
- 40 Takahashi Y, Nagata T, Ishii Y, *et al*. Up-regulation of vitamin D3 up-regulated protein 1 gene in response to 5-fluorouracil in colon carcinoma SW620. *Oncol Rep* 2002;9:75–79.
- 41 Han S, Jeon J, Ju H, *et al*. VDUP1 upregulated by TGF- β 1 and 1,25-dihydroxyvitamin D3 inhibits tumor cell growth by blocking cell-cycle progression. *Oncogene* 2003;22:4035–4046.
- 42 Young L, Yang X, Voigt J. Alteration of gene expression in rat mammary tumors induced by N-methyl-N-nitrosourea. *Mol Carcinog* 1996;15:251–260.
- 43 Desagher S, Martinou J. Mitochondria as the central control point of apoptosis. *Trends Cell Biol* 2000;10:369–377.
- 44 Rhodin JAG. *Histology: A Text and Atlas*. Oxford University Press: New York, 1974.
- 45 Miyaura C, Abe E, Kuribayashi T, *et al*. 1 α , 25-Dihydroxyvitamin D3 induces differentiation of human myeloid leukemia cells. *Biochem Biophys Res Commun* 1981;102:937–943.
- 46 Hewison M, Zehnder D, Bland R, *et al*. 1 α -Hydroxylase and the action of vitamin D. *J Mol Endocrinol* 2000;25:141–148.
- 47 Hui T, Sheth S, Diffley J, *et al*. Mice lacking thioredoxin interacting protein provide evidence linking cellular redox state to appropriate response to nutritional signals. *J Biol Chem* 2004;279:24387–24393.
- 48 Schulze P, Yoshioka J, Takahashi T, *et al*. Hyperglycemia promotes oxidative stress through inhibition of thioredoxin function by thioredoxin-interacting protein. *J Biol Chem* 2004;279:30369–30374.
- 49 Nishinaka Y, Masutani H, Oka S, *et al*. Importin α 1 (Rch1) mediates nuclear translocation of thioredoxin-binding protein-2/vitamin D3-up-regulated protein 1. *J Biol Chem* 2004;279:37559–37565.
- 50 Butler L, Zhou X, Xu W, *et al*. The histone deacetylase inhibitor SAHA arrests cancer cell growth, up-regulates thioredoxin-binding protein-2, and down-regulates thioredoxin. *Proc Natl Acad Sci USA* 2002;99:11700–11705.
- 51 Hamazaki S, Okada S, Ebina Y, *et al*. Nephrotoxicity of ferric nitrilotriacetate. An electron-microscopic and metabolic study. *Am J Pathol* 1986;123:343–350.